의학박사 학위논문

Deciphering the mechanism of glioblastoma recurrence driven by mutation-harboring neural stem cell

교모세포종에서 돌연변이를 갖는
신경줄기세포 기원의
재발 기전 연구

2023년 8월

서울대학교 대학원
의학과 방사선종양학 전공
리 슈 에

Deciphering the mechanism of glioblastoma recurrence driven by mutation-harboring neural stem cell

Thesis director Hong-Gyun Wu

Submitting a Ph.D. Dissertation of Medicine

April 2023

Graduate School of Medicine
Seoul National University
Radiation Oncology Major

Li Xue

Confirming the Ph.D. Dissertation is written by
Li Xue
July 2023

Chair _____(Seal)

Vice Chair _____(Seal)

Examiner _____(Seal)

Examiner _____(Seal)

Examiner _____(Seal)

Abstract

Deciphering the mechanism of glioblastoma recurrence driven by mutation-harboring neural stem cell

Li Xue

Medicine (Radiation Oncology Major)

The Graduate School

Seoul National University

Introduction: Glioblastoma (GBM) is a highly malignant primary brain tumor with a poor prognosis. The current standard of care involves maximal surgical resection, radiation therapy, and temozolomide (TMZ). Despite complete resection, about 85% of recurrences are observed in the resection margin, indicating the need for more effective treatments. Recent research suggests that neural stem cells (NSCs) located in the subventricular zone (SVZ) may be the cell of origin for GBM. The involvement of NSCs in tumor recurrence remains unclear, and therapy involving radiation to the SVZ has been proposed to prevent tumor recurrence. Therefore, further investigation is required to elucidate the molecular and cellular mechanisms underlying the contribution of NSCs to GBM recurrence.

Methods: To investigate the role of cancer-driving mutant NSCs in the SVZ in glioblastoma, a genetically modified mouse model of surgical resection was generated. Cancer mutations, including EGFR, TP53, and PTEN, were introduced by in vivo electroporation. Tissues from this model were subject to immunohistochemistry and RNA sequencing. Differentially expressed

genes and pathways were investigated and validated using human patient brain tissues. Further biological functions were examined in vivo and in vitro.

Results： The results showed that after SVZ NSCs were subject to surgical resection with somatic genetic events, these cancer-mutant NSCs were redirected specifically towards the resection cavity (RC) through the aberrant growth of oligodendrocyte-precursor cells (OPCs). Furthermore, SVZ mutant NSCs constituted GBM around RC at four weeks post-resection in 64.7% (11/17) of mice. Bulk RNA sequencing of time-course tissues around RC consisting of the normal cortex two days, two weeks after resection, and recurrent tumor samples in mice revealed that the expression levels of CXCR4 were elevated two days after resection and remained high until glioma development. Moreover, the CXCL12/CXCR4 chemokine axis was up-regulated during the migration from the SVZ and tumor formation at the RC compared with primary tumors without the RC in mouse models. Matched primary and recurrent tumor samples from 56 GBM patients showed higher CXCR4 expression levels between local recurrence around the resection cavity after gross total resection without any residual tumor evidence (LR) compared with other recurrent patterns (PD) (P=0.0176), including the progression of residual tumor after incomplete resection and distant intracranial metastasis subgroups. Moreover, high expression level of CXCR4 predicted poor prognosis of LR patients (P=0.018). Blockade of the CXCL12/CXCR4 axis led to a reduction in the number of migrating oligodendrocyte progenitor cells (OPCs) and improved tumor control and survival rates.

Conclusions: Mutated residual NSCs in the SVZ may cause tumor recurrence after surgical removal of primary GBM and the CXCL12/CXCR4 pathway may be a treatment target in post-resection recurrence.

Keywords: Glioblastoma, Neural stem cell, Recurrence, Oligodendrocyte-precursor cells, C-X-C chemokine receptor type 4, Subventricular zone

Student Number: 2018-35031

Table of Contents

Chapter 1. Introduction

1.1. Glioblastoma

Glioblastoma (GBM) is the most aggressive diffuse glioma, accounting for 54% of all gliomas and 16% of all primary brain tumors(2). Several risk factors have been identified for glioblastoma, although most cases occur in people with no known risk factors. Some of the established risk factors for glioblastoma include a family history of brain tumors, exposure to ionizing radiation, and certain genetic syndromes such as neurofibromatosis type 1 (NF1) and Li-Fraumeni syndrome(3).

Currently, there are no curative treatment strategies for GBM. For now, the standard of care for newly diagnosed GBM involves gross total surgical resection (GTR) followed by radiotherapy along with concurrent chemotherapy with temozolomide (TMZ) for six weeks and adjuvant chemotherapy with TMZ for six cycles(4, 5).

Despite advances in diagnosis and treatment, the prognosis of patients with GBM has not improved over the past few years, with a median survival of only approximately 15 months from diagnosis(4, 6).

Even with conventional treatment and supra-total resection, these patients still cannot slip away from recurrence, with a near 100% relapse rate(7, 8). In approximately 80% of aggressively treated patients, disease progression/recurrence occurs within 2 cm of the resection margin(9, 10). Thus, an improved understanding of the factors associated with GBM recurrence can help to inform prevention strategies and improve outcomes for these patients.

1.2. Origin of glioblastoma

One of the factors associated with GBM recurrence is residual mutant neural stem cells (NSCs) in subventricular zone (SVZ), which was previously proved as the cell of origin of GBM[11-13]. Understanding the pathophysiological role of these cells in GBM recurrence is critical to

develop more effective therapies, prevent recurrence, and improve patient survivals.

After the repeated continuous efforts to treat the tumor itself, the origin of GBM emerged as the next generation target(11-13). One of the dominant hypotheses about the existence of the cell-of-origin in GBM is that GBM originates from NSCs residing in SVZ(13-15).

Epidermal growth factor receptor (EGFR) amplification and PTEN loss are causes of primary GBMs(16). Other common theories for the pathogenesis of GBM include the inactivation of TP53(17), PTEN(18), and mutations in telomerase reverse transcriptase (TERT)(19, 20). Each of these genes is known to play a role in the regulation of the SVZ NSCs(21). In the SVZ, epidermal growth factor (EGF) promotes proliferation while preventing NSC differentiation(22-24). Because of the EGFR gene's function in the SVZ, amplification of the EGFR gene has been suggested as a potential mechanism for the development of GBM(21, 25).

PTEN and TP53 are both tumor suppressor genes. GBM frequently has mutations in the gene TP53, which controls cell division, differentiation, and proliferation in the SVZ(16, 17, 26, 27). For NSCs in the SVZ, PTEN controls migration, apoptosis, and proliferation(28, 29). TP53 or PTEN knockout induces a predisposition for neoplastic transformation(18, 30). Telomerase expression in adult mammals is confirmed in the SVZ(31), where it promotes NSC proliferation and survival(32).

Additional components and pathways that are frequently altered in GBM and SVZ include c-Met, FoxO3, the Wnt pathway, and the sonic hedgehog pathway(33, 34). These modifications provide persuasive evidence that SVZ NSCs are the cause of GBM in humans and suggest pathways that can be therapeutically targeted. c-Met, FoxO3, the Wnt pathway, and the sonic hedgehog pathway are some additional elements and pathways that are frequently changed in GBM and SVZ(21, 28-30, 33-35). These alterations highlight pathways that can be therapeutically targeted and offer compelling evidence that SVZ NSCs are the source of GBM in humans.

Recently, Lee et al. (13) described direct molecular genetic evidence from

human patients with GBM and genome-edited mouse models. They performed deep sequencing of triple-matched tissues, including tumor-free SVZ, tumor mass, and normal cortical tissue (or blood), from 28 patients with isocitrate dehydrogenase (IDH) wild-type GBM or other types of brain tumor. Given that the accumulation of somatic mutations, has been implicated in gliomagenesis, they found that normal SVZ tissue away from the tumor in 56.3% of patients with wild-type IDH GBM carrying low-level GBM driver mutations that were observed at high levels in their matching tumor samples. Moreover, by single-cell sequencing and laser microdissection analysis of human patient brain tissue and genome-edited mouse with cancer-mutated NSCs in SVZ of EGFR, PTEN, and TP53 mutations, they found that astrocyte-like NSCs that contain driver mutations migrate from the SVZ and lead to the development of high-grade malignant gliomas in distant brain regions. Conclusively, these results show that NSCs in human SVZ tissue are the cells of origin that contain the driver mutations of GBM.

1.3. Neural stem cells in SVZ as origin of glioblastoma recurrence

Watts group (36) recently performed whole-exome sequencing of 69 multi-region specimens by 5-ALA fluorescence-guided resection from 11 patients, including the tumor mass, SVZ and infiltrative margin areas, as well as matched blood samples. They leveraged phylogenomic approach to dissect the spatio-temporal evolution of each tumor to understand the link between subclones in the main tumor mass and in residual disease left behind in the surrounding brain parenchyma and SVZ following surgery. They found that in 6/11 patients, the SVZ appeared as an early ancestor. Accordingly, these genomic data revealed that residual ancestral disease presenting in the SVZ could be the source of the inevitable relapse that occurs in GBM patients, because of an inherent ability to seed re-growth.

Recent research carried out by Trevor J. Pugh group (37) applied scRNA-seq and genome-wide CRISPR–Cas9 screening to glioblastoma stem cells

(GSCs) cultured from primary tumors of 26 patients with GBM. These approaches characterized a transcriptional gradient spanning two cellular states, including normal neural development and inflammatory wound response within these rare populations. The results showed that established founder somatic copy-number alterations, such as chromosomes 7 and 10, maybe a key factor for the malignant transformation of astrocyte-like NSCs to GSCs.

In summary, exploring the unknown mechanism of local recurrence from NSCs after surgical resection of GBM will be critical for optimizing the treatment of glioblastoma patients in the future.

1.4. Purpose of research

The precise pathological implications of pre-cancerous tumor-initiating NSCs in the SVZ with respect to the development of locally recurrent tumors following surgical resection remain unclear. Therefore, the present study postulated that NSCs harboring mutations in the SVZ might potentially serve as the origin of tumor construction in the resection cavity subsequent to the complete excision of the primary tumor.

Chapter 2. Materials and methods

2.1 Mouse modeling

2.1.1 Cre-expressing constructs to model p53, Pten mutations

AAV:ITR-U6-sgRNA(backbone)-pCBh-Cre-WPRE-hGHpA-ITR was a gift from Feng Zhang (Addgene plasmid # 60229 ; http://n2t.net/addgene:60229 ; RRID:Addgene_60229). pAAV-U6sgp53-U6sgbbSapI-GFAPCre was a gift from Sidi Chen (Addgene plasmid # 100275 ; http://n2t.net/addgene:100275 ; RRID:Addgene_100275). gRNAs targeting p53 (sgP53) and Pten (sgPTEN) were designed as previously described(38).The sequence of targeting sgRNA was listed: sgP53 5'-TAATAGCTCCTGCATGG-3', sgPTEN 5'-GGTCAAGATCTTCACAGA-3'. Oligonucleotides containing each sgRNA sequence were synthesized (Cosmogenetech) and annealed in vitro with a thermocycler.

To generate a single vector containing sgRNAs targeting p53, Pten and pGFAP, Cre recombinase, we amplified GFAP from pAAV-U6sgp53-U6sgbbSapI-GFAPCre plasmid, and then switched pCBh to GFAP in the pU6-sgRNA(backbone)-pCBh-Cre-WPRE-hGHpA plasmid. Next, we amplified pU6-sgP53, pU6-sgPTEN and switched pU6-sgRNA(backbone)_pGFAP-Cre-WPRE-hGHpA to pU6-sgP53-pU6-sgPTEN_pGFAP-Cre-WPRE-hGHpA plasmid (sgTP-GFAP-cre). In addition, we inserted U6-sgRNA(backbone)_pGFAP-Cre-WPRE-hGHpA plasmid to generate sgLacz-pGFAP-Cre.

2.1.2 Mouse care and information

All experiments were approved by the Institutional Animal Care and Use Committee in Seoul National University Hospital (SNUH-IACUC), and animals were maintained in the facility accredited AAALAC International (#001169) in accordance with Guide for the Care and Use of Laboratory Animals 8th edition, NRC (2010). LSL-tdTomato (007914), LSL-Cas9

(25263330) 33 and LSL-EGFRviii (19196966) mice(39) were purchased from the Jackson laboratory, maintained on a C57BL/6 strain and FVB strain background. They were housed in isolator cages with free access to food and water in a quiet room until use. The housing room was located in a specific-pathogen-free condition maintained at a controlled temperature of 23 °C on a split light–dark cycle with lights on at 08:00 and off at 20:00. A routine examination of health status of mice was conducted by the veterinarians and investigators. Disease-specific survival endpoint was met when the mice died or met the criteria for euthanasia under the IACUC protocol. The criteria for euthanasia were: (i) severe weight loss of more than 20%, (ii) severe neurological impairment including paralysis, seizure and hunched posture with impaired motor power, or (iii) head bulging sign.

2.1.3 In vivo electroporation

Postnatal day 0 (P0)-P2 mice pups were anesthetized on ice for over 5 min. The injection site was defined as the middle of a virtual line connecting the lambda and the upper-left corner of the eye. Mouth-controlled microinjection capillary was assembled and use. The tip of the capillary was labelled with a water-resistant oily marker pen to see it easily. The volume of the injected solution was measured by lines drawn every 1μL on the capillary. The capillary was slowly lowered 4 mm down into the right lateral ventricle. One μl of plasmid solution supplemented with “1% Fast Green” dye was injected by applying constant and controlled pressure by mouth. The capillary was retracted 5 s after the end of the injection. Correct plasmid injection was monitored by visualizing the outline of the dye-filled lateral ventricle through the skull. After being successfully injected, 5-mm tweezer electrodes (45-0489, BTX-Harvard apparatus) were positioned on each side of the head and applied with five electrical pulses (100 V, 50 ms duration, 950 ms intervals) using the ECM830 electroporator (BTX-Harvard apparatus). After electroporation, pups were placed on a 37 °C heating pad until they started to move and were returned to their mother.

2.1.4 Surgical resection

For surgical resection, four-week-old mice were anesthetized by intraperitoneal injection of a mixture of ketamine and xylazine and positioned in a stereotaxic frame (Stoelting). Following a longitudinal skin incision, a 2 mm diameter craniotomy was made by a hand-held drill, centered at 2 mm posterior to bregma and 2 mm lateral to the midline. Cortical injury was performed with a flat, pipette tip attached to the pump (VACUSIP, INTEGRA Biosciences), with the corpus callosum left intact. After the resection, mice were placed on a 37 °C heating plate until they fully recovered and were returned to their cages.

2.1.5 Stereotaxic injection of virus into cortex after surgical resection

To construct adeno-associated virus (AAV) targeting astrocytes, we co-transfected pAAV5 capsid plasmid, virus assembly helper plasmid (pAd deltaF6, purchased from UPENN Vector Core), and target plasmids to HEK293T cells using polyethylenimine (1 mg ml^{-1}). Before transfection, fetal bovine serum (FBS; Gibco)-containing DMEM (Gibco) was replaced with serum-free media. Six hours after transfection, the media was replaced again with FBS-containing DMEM. Transfected cells were incubated for 72 h. Collected cells were re-suspended in 50% fresh DMEM and 0.04% DNase I (Worthington) in nuclease-free water and then lysed with a series of three freeze and thaw cycles. Cellular debris and AAV-containing supernatant were segregated by centrifugation, and supernatant was collected. AAV was collected by polyethylene glycol-mediated purification(40).

For stereotaxic injection, four-week-old mice were anaesthetized by intraperitoneal injection of mixture with ketamine and xylazine, and positioned in a stereotaxic frame (Stoelting). Hamilton syringe were inserted through the hole using the stereotaxic apparatus and positioned unilaterally at the surface of the brain. One hundred nl of virus solution at a

flow rate of 25 nl min−1 was injected using a syringe pump (KD Scientific Inc.). After the injection, the syringe was retracted slowly after 3 min. We performed virus injection at the margin of resection cavity immediately after surgical resection or 2 weeks before surgical resection. Coordinates for injections before surgery were 0.8, -1 and -1 (in mm: caudal, lateral and ventral to bregma). After the injection, mice were placed on a 37 °C heating pad until they fully recovered and were returned to their cages.

2.1.6 In vivo treatment with AMD3100

CXCL12/CXCR4 chemokine axis was pharmaceutically blocked using Plerixafor (AMD3100, Sigma, A5602), a specific CXCR4 blocker. Following surgical resection, mice were injected with AMD3100 (1.25 mg/kg) or PBS intraperitoneally twice per day (with an interval of 6 h between two injections). After the final injection, mice were sacrificed and brains were harvested.

2.1.7 Sphere culture

GBM tumorsphere (tumorshpere) were generated from tumors induced in LSL-EGFRviii f/+; LSL-tdTomato f/+ mice using the pU6-sgP53-pU6-sgPTEN_CBh-Cas9-P2A-Cre plasmid and were grown as tumorsphere in Neural Stem cell media: DMEM/F12 (Corning, 0-090-CV) supplemented with B27 (50X, Gibco, 17504044), Penicillin-Streptomycin(Gibco, 15140122), and recombinant human EGF (Novoprotein, C046) and bFGF(Novoprotein, C029) at a final concentration of 20ng/ml, respectively. To maintain the cell lines, tumorsphere were dissociated with Accutase (Gibco, A1110501), plated at a density of 2 x 105 /ml and passaged every 4-5 days.

SVZ sphere (neurosphere) were generated from mutated SVZ induced in LSL-EGFRviii f/+; LSL-Cas9-GFP f/+ mice using the pU6-sgP53-pU6-sgPTEN_pGFAP-Cre-WPRE-hGHpA plasmid and cultured as neurosphere in Neural Stem cell media. They were maintained as described above.

2.1.8 Orthotopic implantation and surgical removal primary tumors

tdTomato+ tumorshpere cells derived from LSL-EGFRviii f/+; LSL-tdTomato f/+ mice were orthotopically implanted into three week-old LSL-EGFRviii f/+; LSL-Cas9-GFP f/+ mice, which were previously injected with sgTP-GFAP-cre plasmid and conducted by electroporation at P0-2.

At three to four days culture, tdTomato+ tumorsphere cells were collected and dissociated to a single cell suspension. Cells were re-suspended in a small volume of plain DMEM/F12 to a concentration of 1 x 105 cells/ul and then 1 ul of them were stereotaxically injected into the cortex of LSL-EGFRviii f/+; LSL-Cas9-GFP f/+ mice. After one week of growth, bulky primary tumor developed and were removed by surgical resection as described above. Mice were monitored daily for signs of tumor burden. Moribund mice were sacrificed and brains were processed for histological analysis.

2.2 Immunostaining and histological analysis of mouse brain

Mice at each condition were sacrificed and perfused. Brains were then harvested and fixed in freshly prepared phosphate-buffered 4% paraformaldehyde (4% PFA), cryoprotected overnight in 30% buffered sucrose, and made into O.C.T compound (3801480, Leica Biosystems)-embedded frozen blocks stored at −80 °C. Cryostat-cut sections (25-μm thick) were collected and placed on glass slides. For H&E staining, cryostat-cut sections were collected at a thickness of 4 μm. The slides were then stained with the following antibodies: Mouse antibody to Nestin (1:200 dilution; MAB5326, Merck Millipore), rabbit antibody to GFAP (1:500 dilution; Z0334, DAKO), rabbit antibody to oligodendrocyte transcription factor 2 (OLIG2; 1:500 dilution; AB9610, Merck Millipore), rat antibody to platelet-derived growth factor receptor α (PDGFRα; 1:200 dilution; 14-4321, eBioscience), rabbit antibody to S100β (1:500 dilution; ab52642, Abcam),

rat antibody to myelin basic protein (MBP; 1:500 dilution; MAB386, Merck Millipore), rabbit antibody to Ki67 (1:500 dilution; ab15580, Abcam), rabbit antibody to NeuN (1:500 dilution; ab104225, Abcam), mouse antibody to C※C chemokine receptor type 4 (CXCR4; 1:500 dilution; sc-53534, Santa Cruz Biotechnology), rabbit polyclonal antibody to CXCL12 (1:500 dilution; ab25117, Abcam), mouse antibody to IBA1 (1:500 dilution; GTX632426, Genntex). DAPI included in mounting solution (P36931, ThermoFisher) was used for nuclear staining. We obtained images using a Zeiss LSM800 confocal microscope with Z stacks by step size 1.5 μm. Fluorescence intensities reflecting the distribution of fluorescent reporter-positive cells were converted into grey values and measured using ImageJ software (http://rsbweb.nih.gov/ij/).

2.3 MRI imaging of mouse brain

The mice were first put to sleep by breathing in 5% isoflurane in a mixture of air and oxygen, and they were then put in a cradle for MRI scans while wearing a respiratory mask attached to 1.5% isoflurane in a mixture of air and oxygen. A birdcage mouse head coil was used in MRI investigations using a 3T MRS 3000 scanner (MR Solutions). T1-weighted and T2-weighted images were respectively acquired with spin echo (SE) and fast spin echo (FSE) sequences for investigation of anatomical and pathological conditions. These scan parameters were used: time to repeat/echo time = 550/11 ms (SE) and 3,000/68 ms (FSE), field of view = 22 × 22 mm2, matrix size = 256 × 256 (SE) and 256 × 248 (FSE), slice thickness = 1 mm, number of slices = 19, and scan time = 9 min 23 s (SE) and 9 min 18 s (FSE).

2.4 In vitro differentiation analysis treated with AMD3100

For neurosphere differentiation analysis, cells were dissociated with Accutase, plated with a density of 40000 cells per each dish (precoated

with 20 μg/mL Poly-L-ornithine and 10 μg/mL Laminin, Sigma, L2020 and P4957) in Neural Stem cell media with a lower concentration of Fetal bovine serum (FBS, 1%). AMD3100 (25 μM) or PBS was supplemented into cells (with triplicate) every 72h. After 7 days of treatment, cells were immune-stained and processed for analysis of lineage differentiation.

2.5 RNA sequencing

2.5.1 RNA sequencing sampling from mice tissue

Mouse brain tissue samples were quickly flash-frozen in liquid nitrogen after dissection and stored at a temperature of -80℃ to maintain their integrity. The extraction of RNA from the tissue samples was done using the micro RNeasy kit manufactured by QIAGEN, which is widely recognized for its high efficiency and quality.

2.5.2 RNA sequencing sampling from human tissue

The frozen brain tissue samples from patients with primary and recurrent GBM were carefully processed and analyzed to obtain valuable insights into the underlying mechanisms of the disease. After dissection, the tissue samples were quickly flash-frozen in liquid nitrogen and stored at a temperature of -80℃ to maintain their integrity. The extraction of RNA from the tissue samples was done using the micro RNeasy kit manufactured by QIAGEN, which is widely recognized for its high efficiency and quality.

2.5.3 RNA sequencing analysis

To facilitate the sequencing and analysis of the RNA-seq data, cDNA synthesis, library preparation, and sequencing were performed by the experienced technicians at Macrogen. The Novoseq 6000 instrument manufactured by Illumina was used, and 80 million reads were obtained for each sample (40 million in each direction). The paired-end reads were aligned to the UCSC hg38 for human and mm10 for mouse as reference using HISAT2 (v.2.2.0)(41), and the gencode gtf annotation file was used

for annotation.

The quantification of gene expression was calculated using featureCounts from Subread (v1.6.4)(42) on each genome-mapped read file. The cell count files were merged into a matrix using a homemade python script (Python 3.6), and the raw read counts were used for further analysis. The data was filtered for genes that had at least ten counts across all samples.

DESeq2 (v.1.22.2)(43) was then used to calculate the size factors for each sample and perform variance stabilizing transformation. A batch correction was performed to incorporate technical and biologically relevant features into the model. The variance stabilizing-transformed bulk RNA-seq data were used as inputs for clustering. Differential gene expression analysis was carried out using DESeq2, and batch status was incorporated as a covariate in the expression model. Up-regulated genes were defined as those with a Log2Fold Change greater than 1 and an FDR less than 0.01. Gene set enrichment analysis (GSEA) (v.3.0)(44) was performed on genes ranked by differential expression, and the pathways used for GSEA were obtained from the Molecular Signatures Database (MSigDB). The pathways were filtered for those with a minimum size of 15 and a maximum size of 500 genes.

The R package “clusterProfiler” (v3.10.1)(45) was used to conduct gene set enrichment analysis (GSEA) of the Gene Ontology (GO) to compare the biological processes (BP), cellular components (CC), and molecular functions (MF) of the differentially expressed genes (DEGs). The five most significant biological processes in the results were shown, with an FDR less than 0.05 and a log2FC less than or equal to 1. Additionally, the Kyoto Encyclopedia of Genes and Genomes (KEGG) pathway enrichment analysis of DEGs was performed using the same package. The results were visualized using bar plots of the top 20 pathways.

2.6 Statistical analysis

Data are presented as a mean ± s.e.m. Results were analyzed with a t-test, Manny-Whitney U test or Fisher’s exact test where appropriate using

GraphPad Prism version 9.4.1 (Graph-Pad Software, Inc.). Tumor accumulated incidence and survival data for mice were analyzed with Kaplan–Meier analysis. All P values less than 0.05 were considered statistically significant. All experiments related to the use of animals or a source of cells were subjected to randomization. Sample sizes were predetermined based on the variability found in preliminary and similar experiments. Researchers were not blinded to allocation during experiments and outcome analysis.

Chapter 4. Results

3.1 Mouse modeling of SVZ-driven glioma at RC after surgical resection

To evaluate the potential of residual NSCs from the SVZ to cause a local relapse of GBM in vivo, we established an in vivo genome editing mouse model through postnatal electroporation of TP53, PTEN, and EGFR mutations into NSCs of the SVZ (Figure 1 A-C). The approach involved injecting a single vector containing Cas9 and Cre recombinase along with specific single guide RNAs (sgRNAs) that efficiently targeted TP53 and PTEN in the confined region of the SVZ. For the control group, sgRNA targeting the LacZ gene was used instead of TP53 and PTEN. We also generated the RC via a cortical resection in a remote cortex region, ensuring that the white matter was not disturbed.

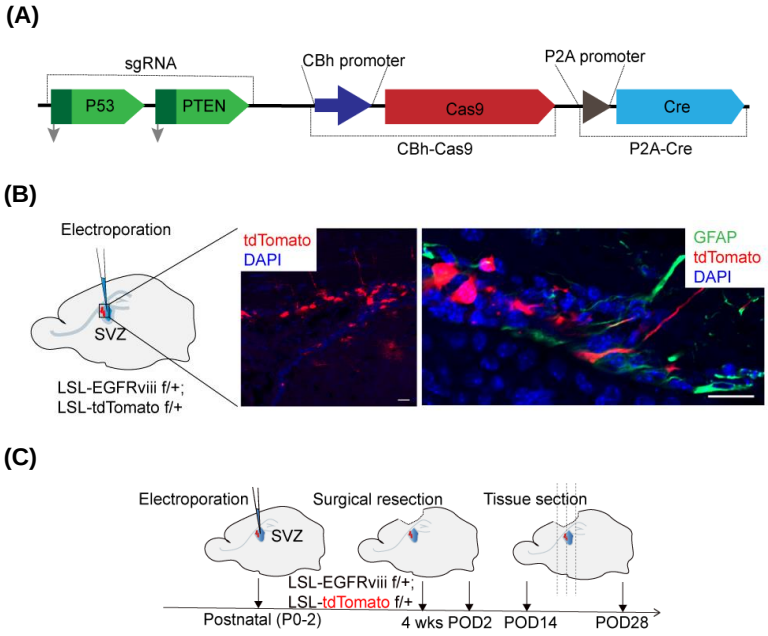

Figure 1. Mouse modeling procedure. (A) Construction of a plasmid containing sgRNA targeting TP53 and PTEN, as well as Cre and Cas9. (B) Electroporation of the plasmid into the SVZ of LSL-EGFRviii f/+; LSL-tdTomato f/+ mice for tracing astrocyte-like NSCs. (C) Surgical resection of

the mouse brain at four weeks after electroporation and tissue dissection on post-operative days (POD2, POD14, and POD28). Scale bars, 20 μm.

3.1.1 Glioma reconstruction at the RC

This model can recapitulate the GBM patients carrying residual mutant NSCs at SVZ after the total removal of primary tumor via surgical resection. The results showed that the tdTomato-positive cells migrated to the RC (Figure 2A-D). Furthermore, 64.7% of the mice (11 out of 17) developed brain tumors around the RC except in other regions four weeks after surgery, while no tumors were observed in control mice (Figure 2A). Histological examination of these tumors through immuno- and Haematoxylin and eosin (H&E) staining revealed that they displayed classical features of highly proliferative, high-grade glioma (Figure 2C). These findings suggest that residual SVZ NSCs with mutations can migrate to the resection site and cause malignant glioma around RC after surgery.

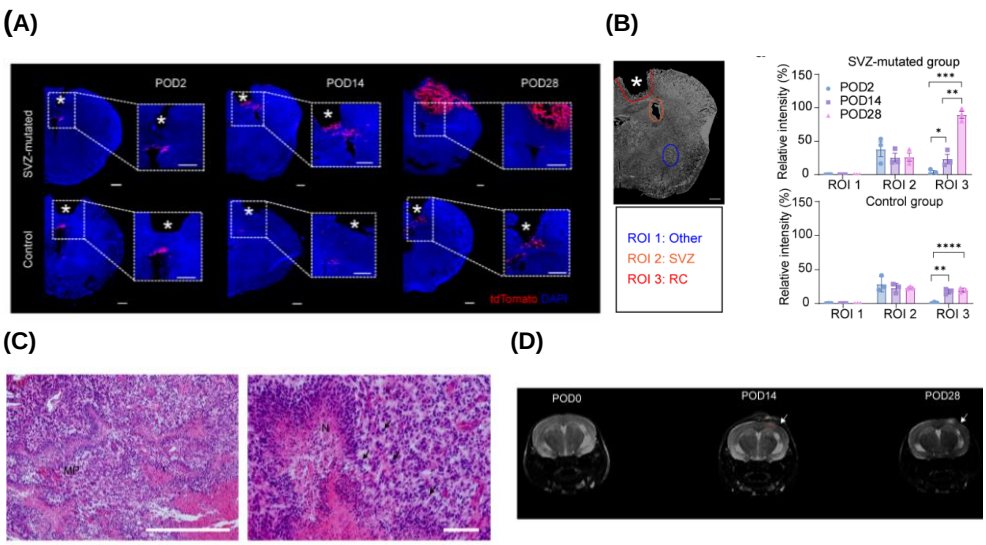

Figure 2. Glioma construction at RC after surgical resection. (A) Representative coronal sections of mice stained with DAPI POD2, 14, and 28 in each group (n=3); the asterisks indicate the RC; images from SVZ-mutated mice showing that the tdTomato-positive cells are initially located in the rostral SVZ, where mutations are edited. Over time, these cells migrate to the RC and proliferate to form the tumor; however, there is no

tumor formation in the control group; scale bars, 500 μm; representative images showing the whole brains of mouse phenotypes; white dashed box indicates the immigration of NSCs to RC. (B) Illustration of the strategy for the measurement of the number of tdTomato-positive cells in different regions; regions of interest (ROIs) 1–3 with blue, carrot orange, and red color are defined as random regions of the cortex except for the SVZ and RC, SVZ and RC, respectively; scale bar, 500 μm. (C) Measurement of tdTomato immunofluorescence intensities (relative to DAPI) at different post-resection time points in ROIs 1–3 of the SVZ-mutated group, compared with those of the control group. ROI 1 was defined as any random area of the brain excluding the SVZ or RC, ROI 2 as the SVZ region, and ROI 3 as the RC site; *p=0.0423, **p=0.0017, **** p<0.0001, (n=3 for control and mutant mice at each time point); the error bars represent the mean ± SEM; one-way ANOVA. (D) Representative MRI imaging of mouse brain at POD2, POD14, and POD28 after surgical resection. The white arrow indicates the resection cavity.

3.1.2 Glioma reconstruction at RC after primary tumor removal

After resection of primary tumors, the recurrent GBM tumor at RC may be attributed to two sources of tumor-initiating cells: residual regrowing tumor cells after incomplete resection of primary tumors around RC following a dormant period or clonal evolution of residual NSCs of SVZ to the tumor around RC. To investigate which of these scenarios is correct, we established a mouse model comprised of two stages and a dual-color reporting system. In the first stage, we transduced the SVZ of LSL-EGFRviii; LSL-Cas9-GFP mice with a plasmid via postnatal electroporation, resulting in GFP-positive NSCs harboring mutations at SVZ. In the second stage, we implanted tdTomato-positive tumor cells into the cortex of the mice and closely monitored the mice for tumor re-growth, and attempted the gross total removal of the tdTomato-positive primary tumor via surgical operation one-week post-implantation. (Figure 3A-B) The tdTomato reporter represents recurrent tumors originating from residual tumor cells of the primary tumor, while the GFP reporter highlights the contribution of SVZ-

mutated NSCs to reconstruct recurrent tumors. Interestingly, 57.1% of the mice (4 out of 7) displayed GFP-positive recurrent tumors at the site of the RC after the removal of the primary tdTomato-positive tumor (Figure 3C). Our results suggest residual NSCs harboring cancer-driving mutations at the SVZ can reconstruct the recurrent GBM tumor after resection of the primary tumor. These findings provide novel insight into the potential mechanisms of GBM recurrence and highlight the importance of further investigation into the role of residual mutant NSCs in the SVZ.

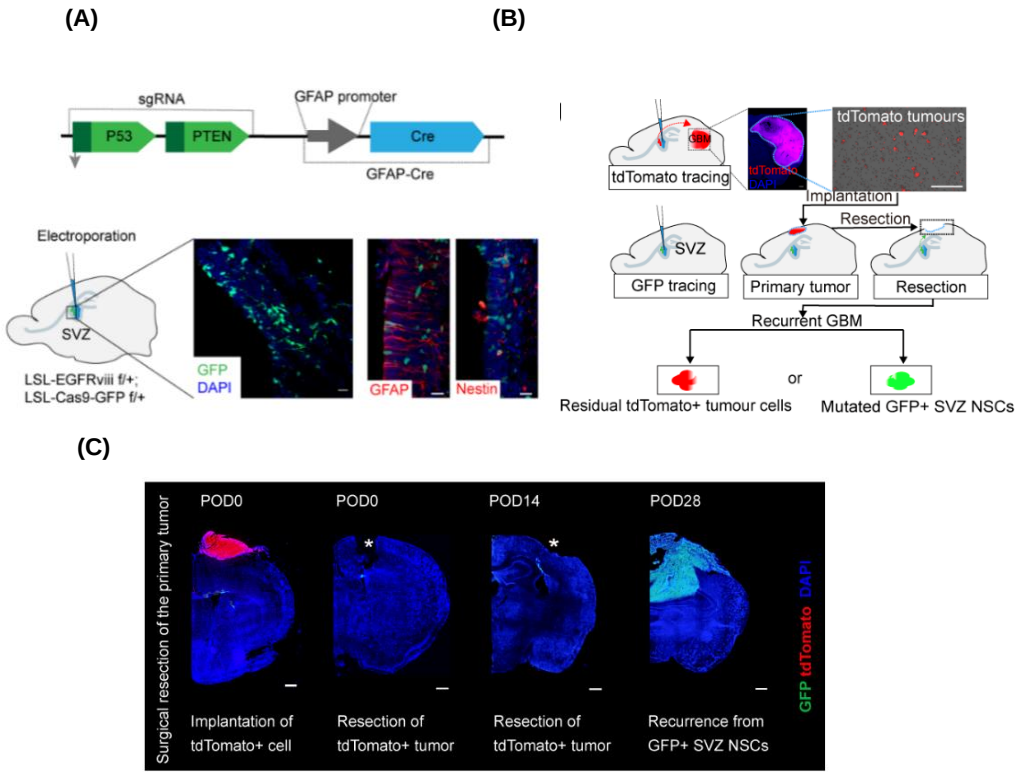

Figure 3. Glioma construction at RC from mutant NSCs after removal of the primary tumor. (A) Mouse modeling of introducing a single plasmid with the GFAP promoter and expressing Cre recombinase with sgRNAs targeting TP53/PTEN into SVZ of LSL-EGFR f/+; LSL-Cas9-GFP f/+ mice. (B) Schematic diagram of transplanted tumor model; first, primary glioblastoma cells were dissected from the brains of mice carrying tdTomato-positive primary tumors and cultured as suspension cells; four weeks after electroporation, these cells were implanted into the cerebral cortex of SVZ-mutated mice; one week later, a bulky tumor formed and was

surgically removed; recurrent tumors in the RC post-resection are shown; in scenario 1 (left), recurrent GBM is shown in red color, indicating that residual tdTomato-positive cells had constructed the RC; in scenario 2 (right), recurrent GBM is shown in green color, suggesting that SVZ cancer-mutated GFP-positive cells may migrate to and evolve into the recurrent tumor at RC. (C) Representative images showing sections from tumor-implanted mice on day seven after implantation and POD0, 14, and 28 of the surgical removal of the primary tumor; scale bars, 500 μm.

3.1.3 Surgical resection and viral transduction of cancer mutation in the cortex

To determine the possibility of whether other sources of distant cortical cells can migrate to RC, we introduced the TP53, PTEN, and EGFR mutations into the RC after surgical resection or into the prefrontal cortex, away from the RC. In both experiments, we observed neither the spread of cells to the SVZ or RC nor significant proliferation of cells, compared to the mouse model harboring driver mutations in SVZ (Figure 4A-F). To rule out the influence of the proximity between the surgical site and SVZ, we performed the surgical resection in the distant caudal brain of the parietotemporal lobe and still observed tumor occurrence at the distant RC, consistent with our previous observations (Figure 4G,4H).

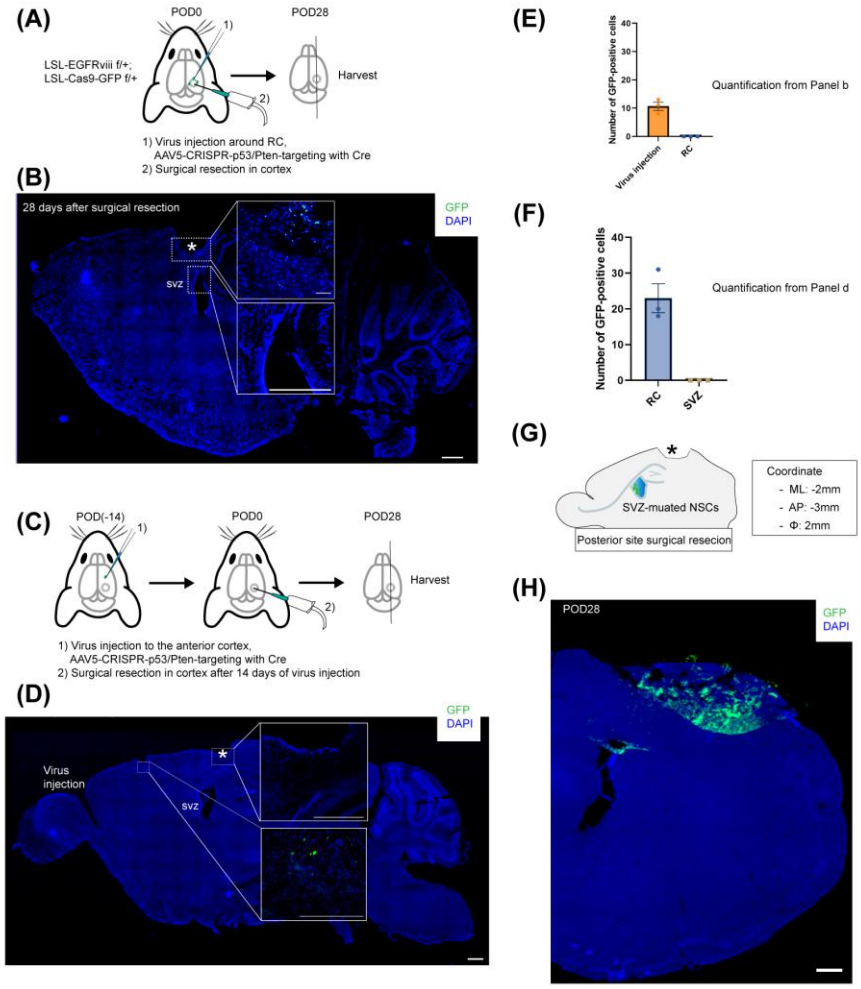

Figure 4. Surgical resection and viral injection targeting driver mutations in the cortex. (A) Experimental scheme showing the procedure of viral injection of AAV5 containing sgRNAs for P53 and Pten genes, with the expression of Cas9 and Cre recombinase in the cortex, followed by surgical resection in 4-week-old LSL-EGFRviii; LSL-Cas9-GFP mice. (B) Representative images showing immigrating cells around the RC (upper panel, scale bar, 20 μm) and ipsilateral SVZ (lower panel, scale bar, 500 μm) 28 days after the procedure in panel a. Scale bar, 500 μm. (C) Experimental scheme showing the procedure of viral injection of AAV5 containing sgRNAs for the P53 and Pten genes, with the expression of Cas9 and Cre recombinase in the cortex, followed by surgical resection after two weeks, in LSL-EGFRviii; LSL-Cas9-GFP mice. (D) Representative images showing immigrating cells around the RC (upper panel) and

injection site (lower panel) 28 days after the procedure in panel c. Scale bars, 500 μm. (E&F), Comparison of GFP-positive cell numbers in the RC, SVZ, and virus injection sites. *p=0.0295 (panel e), *p=0.0181(panel f) (n=3). Student's two-tailed t-test. The error bars represent the mean ± SEM. (G) Illustrations of the experimental procedure for surgical resection of the posterior cortex. (H) Representative images showing local tumor development in the resection site after 28 days of the procedure in panel g. Scale bars, 500 μm.

3.1.4 Mutant NSCs migrating specifically to RC through OPC lineage

Finally, through immunostaining of tdTomato-positive cells at the RC, we confirmed that oligodendrocyte precursor cells (OPCs) were the major cellular subtypes of migrating cells from SVZ to RC (Figure 5A-B). These findings support our hypothesis that mutated NSCs in the SVZ exhibit a preferential migratory behavior and lead to the development of high-grade malignant gliomas in the RC after surgery through the aberrant growth of OPC lineage.

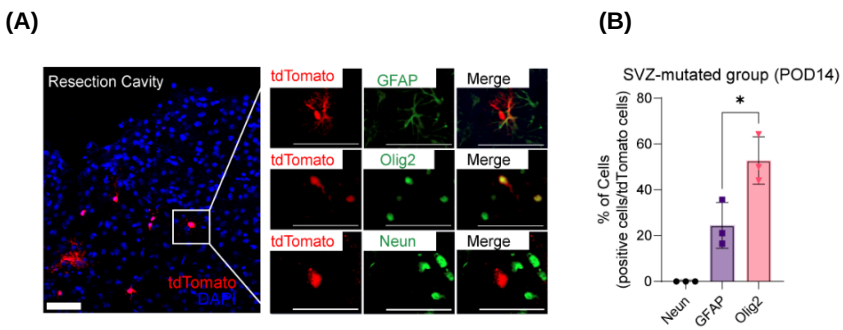

Figure 5. Mutant NSCs were migrating specifically to RC through OPC lineage. (A) DAPI staining image of RC in the cortex on POD14 of surgical resection; mutated cancer cells in the SVZ are tdTomato-positive; scale bar, 20 μm (left panel); representative immunostaining images of GFAP, OLIG2, and NeuN-positive cells colocalized with tdTomato at the RC (right panel); scale bars, 20 μm. (B) Measurement of the percentage of cells positive for various NSC-derived cell lineage markers as shown in panel e; *p=0.0112;

data are shown as the mean ± SEM; two-sided Student's t-test.

3.2 Increased CXCR4 expression at RC after surgical resection

3.2.1 RNA sequencing analysis of RC in mice after surgical resection

Next, we analyzed the temporal transcriptomics at RC to find potential mechanisms and therapeutic targets driving NSCs to evolve into recurrent tumors at RC. The sampling strategy involved collecting samples from the surgical resection cavity and tumors from mice in vivo. Transcriptional changes have been implicated in the progression of glioblastoma. Thus, we focus our attention on genes that were consistent altered in the RC compared with normal cortex using RNA-seq analysis (Figure 6A). We observed 106 co-upregulated genes in time-course samples dissected from RC at post-operative days POD2, POD14, and recurrent tumors, compared to the normal cortex as the control group (Figure 6B).

KEGG analysis revealed one shared pathway among top-ten up-regulated pathways, shown as cytokine cytokine-receptor interaction pathway (a total of 265 genes, Figure 6D). The continuous significant up-regulation of cytokine cytokine-receptor interaction pathway following time after surgical resection was also confirmed by GSEA analysis (Figure 6E).

Finally, there were eight genes that overlapped between significantly co-upregulated genes with ones involved in cytokine cytokine-receptor interaction pathway, including cytokine genes CXCR4, LTBR, CCL22, CCR7, CCL4, CXCL16, TNFRSF1A, and TNFRSF11B). Among these genes, CXCR4 was the top up-regulated gene (Figure 6F) and maintained a continuous up-level trend (Figure 6G).

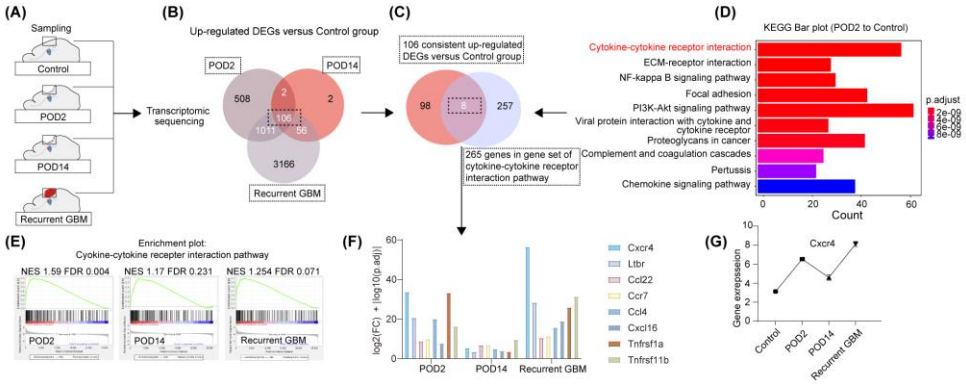

Figure 6. CXCR4 is highly expressed at the RC after surgical resection and correlates with the migration of SVZ-mutated cells. (A) Illustration of the strategy used for sampling mice in the SVZ-mutated group at different timepoints; briefly, the normal cortex, RC, and tumor tissues were dissected for further RNA-sequencing and categorized as the control, POD2 and POD14, and recurrent GBM groups, respectively. (B) Venn diagram showing the overlap between up-regulated DEGs detected via the RNA-seq analysis of post-resection samples from the POD2, POD14, and recurrent GBM group versus the control group samples. (Log2 fold change $\geqslant 1$; adjusted p value $\leqslant 0.01$). (C) Venn diagram showing the overlap between co-upregulated DEGs in the cytokine-cytokine receptor interaction pathway. (D) Bar plot of the KEGG pathway analysis showing the enrichment of up-regulated genes in the POD2 group, compared with those in the control group samples. (E) The cytokine–cytokine receptor interaction pathway enrichment in POD2, POD14, and recurrent GBM groups was determined via gene set enrichment analysis (GSEA), compared to that in the control group; NES, normalized enrichment score. (F) Comparison between the expression levels of eight genes filtered out through panel c among POD2, POD14, and recurrent tumor groups versus control group samples. (G) Measurement of normalized CXCR4 expression levels via time-course transcriptomic profiling.

3.2.2 Immunostaining of CXCR4 and CXCL12 expression in mice

Increased CXCR4 expression level was confirmed by immunohistochemical (IHC) staining of RC and normal cortex (Fig.7A-D). The CXCL12/CXCR4

interaction was found to play a key role in the recurrence of glioma after surgery, as CXCL12 was shown to increase significantly around the RC and recruit CXCR4 positive neural stem cells to the inflamed surgical bed.

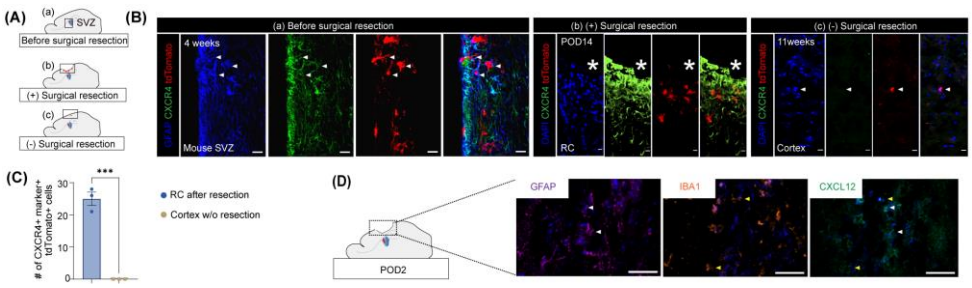

Figure 7. Validation of increased CXCR4 at RC after surgical resection. (A) Illustration of the strategy of sampling mouse SVZ, RC, and cortex in the SVZ-mutated group. (B) Representative immunostaining images of CXCR4 in the mouse SVZ without surgical resection, in RC on POD 14, and in the normal cortex after 11 weeks without surgical resection; Scale bars, 50 μm; the white arrowheads represent CXCR4-positive cells colocalizing with tdTomato-positive cells in the SVZ-mutated group. (C) Measurement of the number of CXCR4-positive tdTomato-positive cells around the RC on POD14 and normal cortex without surgical resection at 8–11 weeks; ***p=0.0003; data shown are as the mean ± SEM; two-sided Student's t-test. (D) Representative immunostaining images of GFAP, IBA1, and CXCL12 in RC on POD2 after surgical resection. The white arrowheads represent GFAP-positive astrocytes colocalizing with CXCL12, and the yellow arrowheads represent IBA1-positive microglia colocalizing with CXCL12. Scale bars, 50 μm.

3.3 Analysis of primary and recurrent tumor tissues in mice and human

3.3.1 RNA sequencing analysis of primary and recurrent tumor in mice

To further confirm the role of CXCR4 in the development of recurrent tumors, we conducted a comparison of the transcriptomes between recurrent GBM and primary murine GBM, which was driven by SVZ-mutated NSCs that had developed spontaneously without undergoing any surgical resection (Figure.9A). The comparison showed that there were 576 up-regulated and 531 down-regulated differentially expressed genes (DEGs) in the recurrent tumors compared to the primary tumor (Figure 8A-D). A gene ontology (GO) analysis revealed that the pathways that participate in cell division were enriched in the recurrent malignancies (chromosome segregation, nuclear division, Figure 8E-H). We made a hypothesis that the CXCR4 pathway may be enhanced in recurrent malignancies based on the aforementioned time-course transcriptome study. In order to address this, the CXCR4 pathway was significantly enriched in recurrent tumors (NES = 1.307, P = 0.085, Figure 9D). We compared the expression levels of the 18 genes implicated in the CXCR4 pathway. The gene for CXCR4 was shown to be highly elevated in recurrent cancers. The CXCR4 gene was considerably increased in recurrent tumors compared to primary ones (P = 0.0094, Figure 9E). Furthermore, IHC labeling revealed a high level of CXCR4 in recurrent tumors (P < 0.0001, Figure 9F-G).

In conclusion, this study demonstrates that the expression of CXCR4 is substantially expressed in the resection cavity after surgical resection and may be correlated with the migration of cells that have acquired cancer mutations. The biological function of CXCR4 in human samples and its function in the migration and recurrence of GBM following surgical resection requires further investigation in order to be fully validated.

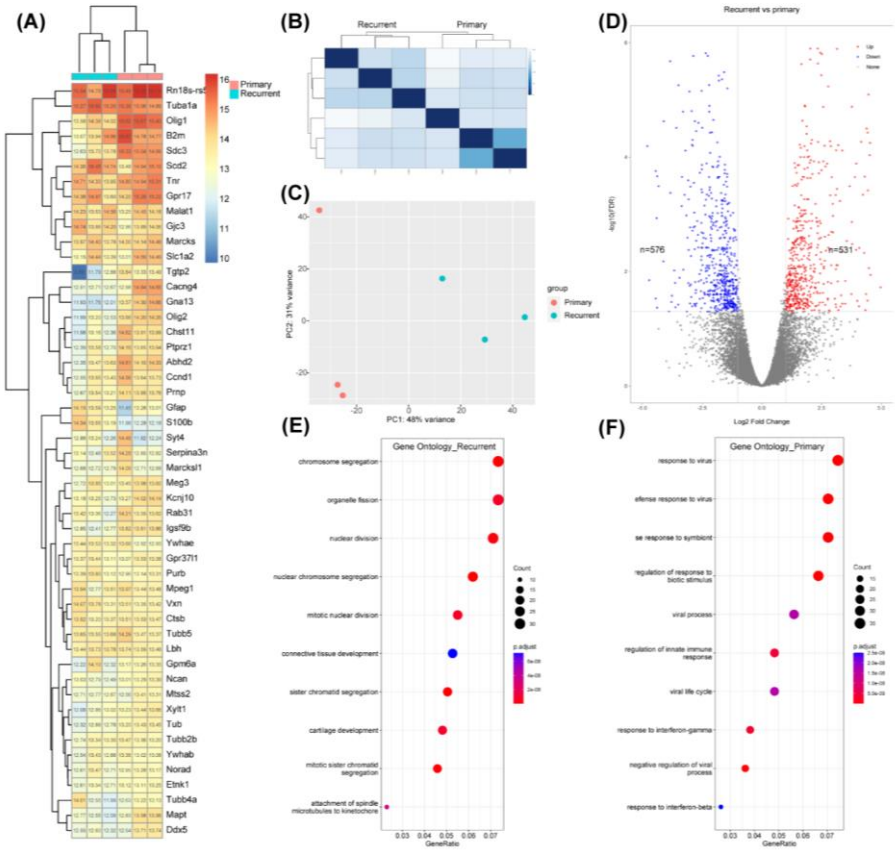

Figure 8. Transcriptome profiling of paired primary and recurrent tumors from mice. (A) Heatmap plot illustration of the top regulated genes in primary and recurrent samples derived from primary and recurrent samples of the mouse model. (B) Heatmap of DEGs between primary and recurrent mouse GBM samples. (C) Principal Component Analysis (PCA) plot of primary and recurrent mouse GBM samples. (D) The volcano plot shows the fold change against the adjusted p-value for genes, as described in the hierarchical cluster analysis. The blue and red dots represent genes with significant changes (FDR<0.05, FC>2). (E&F) Dot plot of the gene ontology analysis enriched in the recurrent and primary samples, respectively.

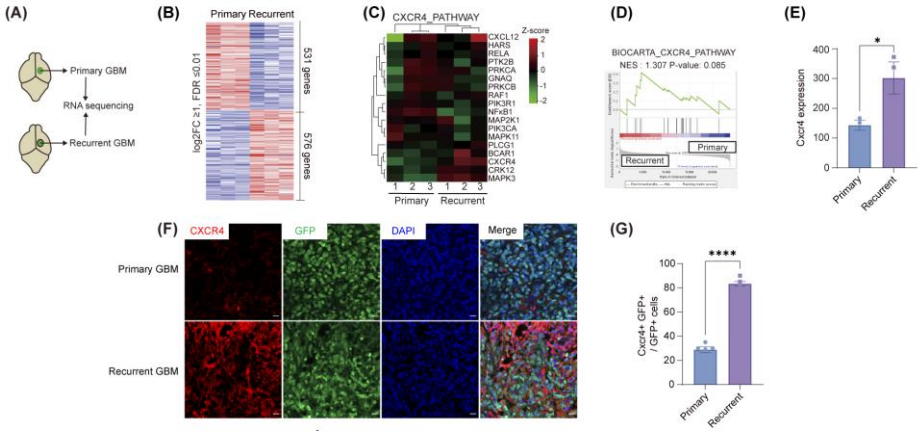

Figure 9. CXCR4 expression in the GBM reconstructed after surgical resection in mice was increased compared to other progressive recurrent diseases. (A) Illustration of primary and recurrent GBM tissues dissected from mice. (B) Heatmap plot of the DEGs of primary and recurrent tumor samples obtained from in vivo mouse models (n=3). (C) Heatmap depicting the expression levels of the 18 signature genes between recurrent and primary tumors (red corresponds to overexpression in recurrent compared to primary samples, and green to overexpression in primary relative to recurrent samples). (D) GSEA of CXCR4 pathway enrichment scores in recurrent tumors compared with those in primary tumors. (E) Comparison of normalized CXCR4 read counts in primary and recurrent GBM tissues from mice; **p=0.0094; the error bars represent the mean ± SEM; two-sided Student's t-test. (F) Immunochemical staining images of CXCR4 expression in primary and recurrent GBM tissues of mice. (G) Measurement of CXCR4 expression levels in each group; **** p<0.0001.

3.3.2 RNA sequencing analysis of primary and recurrent tumor in human

We performed a transcriptional profile analysis on 56 matched primary and recurrent tumor samples from GBM patients to confirm the expression and function of the CXCR4 axis in the local recurrence around RC of human patients (Figure 11A-C, Figure 12). Our analysis identified 446 DEGs, of which 94 were unique to primary GBM, and 352 were significantly elevated in recurrent GBM (Figure 10D, with an adjusted p-value of 0.05 and a 1-fold

change). However, the expression of CXCR4 or CXCR4-related pathway was not elevated in recurrent GBM, compared with matched primary ones (Figure 10E, Figure 11B). This result was consistent with the findings from the study, which analyzed 14 matched human primary-recurrent GBM pairs and found that CXCR4 expression was essentially identical in these samples.

Our in-vivo model recapitulated the local recurrence around RC after complete resection of the primary tumor, which is the dominant pattern of recurrences in the GBM. Therefore, we distinguish the recurrences between local recurrence around the resection cavity after gross total resection without any residual tumor evidence (LR) and the other recurrent patterns (PD), including the progression of residual tumor after incomplete resection and distant intracranial metastasis subgroups (Figure 11C). Transcriptome analysis was utilized to compare gene expression profiles between recurrent tumor specimens from LR and PD patients, with the aim of identifying potential molecular pathways associated with glioblastoma recurrence. The results of this analysis showed that CXCR4 expression levels were higher in recurrent tumor specimens from LR patients compared to those from PD patients (P=0.0176) (Figure 11D). Furthermore, the CXCR4 molecular pathway had a higher enrichment fraction in the LR patient group, suggesting that CXCR4 signaling may also play a role in promoting LR of glioblastoma (Figure 11E). To further explore the clinical significance of CXCR4 expression in glioblastoma, the relationship between CXCR4 expression level and patient prognosis was analyzed. The results showed that patients with high CXCR4 expression had worse overall survival (OS) (P=0.018) (Figure 11G), implicating the prognostic effect of the distinct recurrence pattern. Taken together, these findings suggest that targeting CXCR4 signaling may be a promising therapeutic approach for preventing or reducing LR of glioblastoma. Also, the differential approach to recurrences will be required according to the cellular source and mechanisms of recurrences.

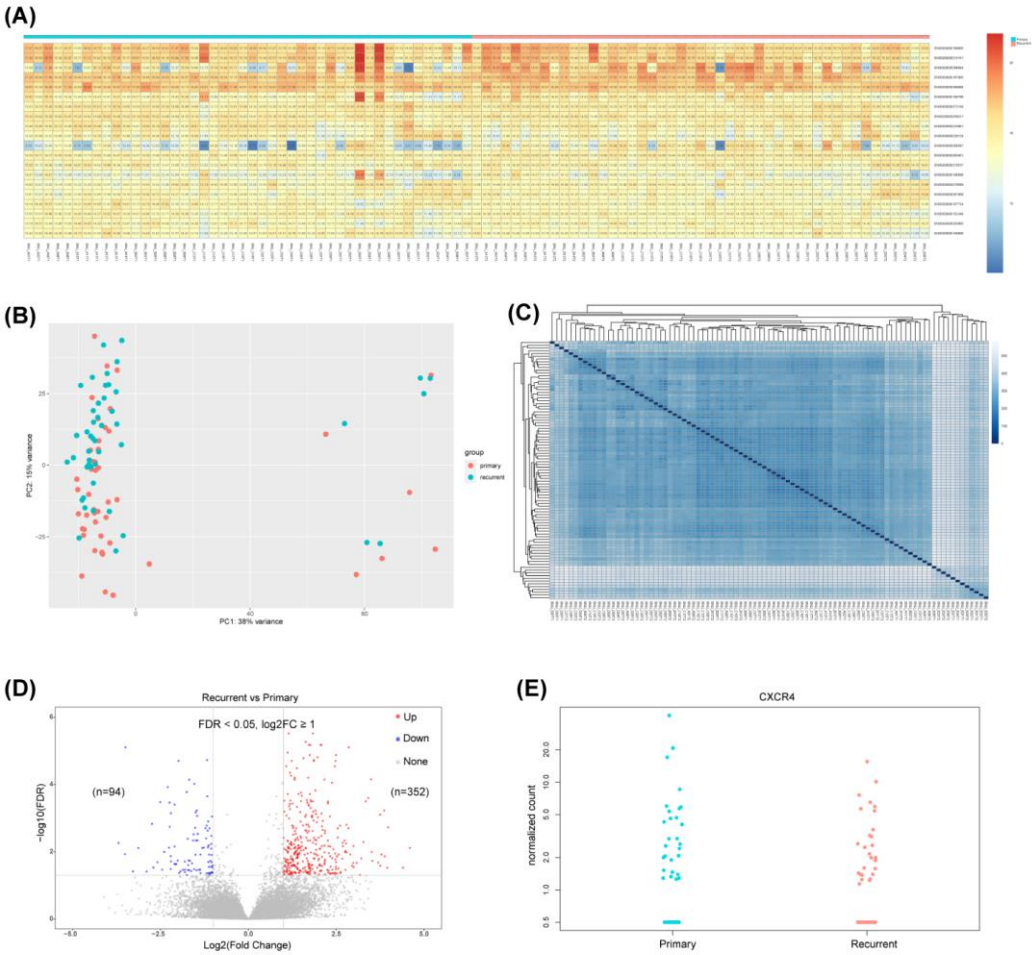

Figure 10. Transcriptome profiling of paired primary and recurrent tumors from humans. (A) Heatmap of DEGs compared between primary and recurrent human GBM samples. (B) Principal Component Analysis (PCA) plot of primary and recurrent human GBM. (C) Hierarchical cluster analysis of 93 human GBMs, including 46 primary and 47 recurrent samples. (D) The volcano plot shows the fold change against the adjusted p-value for genes, as described in the hierarchical cluster analysis. The blue and red dots represent the genes whose levels showed significant changes (FDR<0.05, FC>2). (E) Normalized read counts the level of CXCR4 in the primary and recurrent groups.

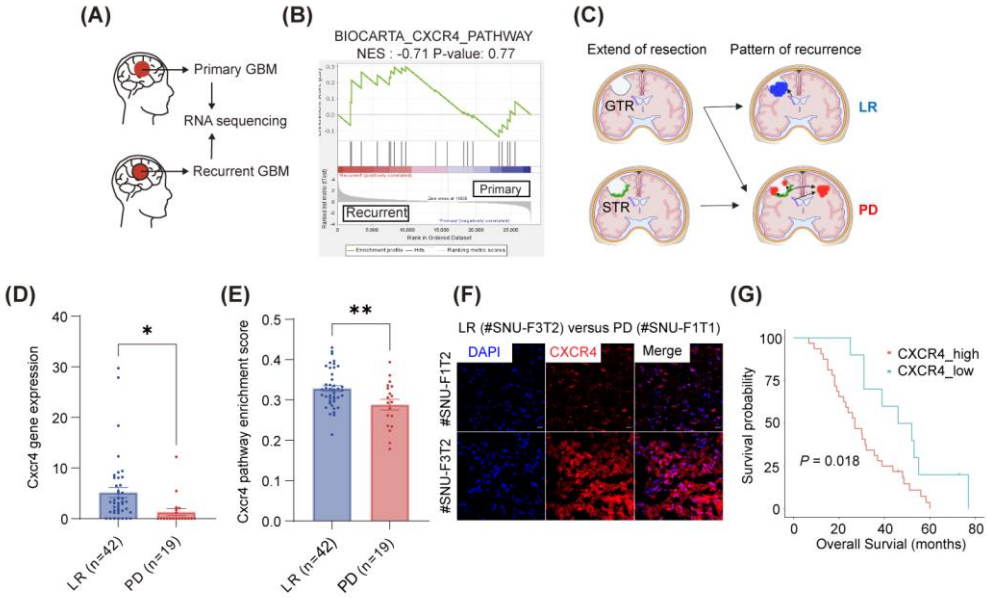

Figure 11. CXCR4 expression in GBM patients with local recurrence was increased compared to progressive recurrent diseases. (A) Illustration of the strategy used for sampling from matched primary and recurrent GBM tissues from human patients. (B) GSEA of the CXCR4 pathway enrichment scores in recurrent tumors, compared to matched primary ones from human patients. (C) Graphical depiction of the LR and PD subgroup. GTR, gross total resection. STR, subtotal resection. SVZ mutated NSCs are represented in purple, and residual tumor cells in green. (D) Comparison between the CXCR4 expression levels of LR and PD tumor samples; *p=0176; the error bars represent the mean ± SEM; two-sided Student's t-test. (E) Comparison between the CXCR4 pathway enrichment scores of LR and PD tumor samples; **p=0063; the error bars represent the mean ± SEM; two-sided Student's t-test. (F Immunochemical staining images of CXCR4 expression in primary and recurrent GBM tissues of humans. #SNU-F3T2 from LR group and #SNU-F1T2 from PD group, respectively. (G) Overall survival graph of recurrent GBM patients in the LR group, compared with that in the PD group, based on CXCR4 expression.

3.3.3 Analysis of CXCR4 expression from public database

To test the validity of our transcriptome data analysis and the results that CXCR4 was not showing significantly elevated in recurrent tumors of humans, we used the public database (GSE139533) to verify this result (Figure 12 A-C).

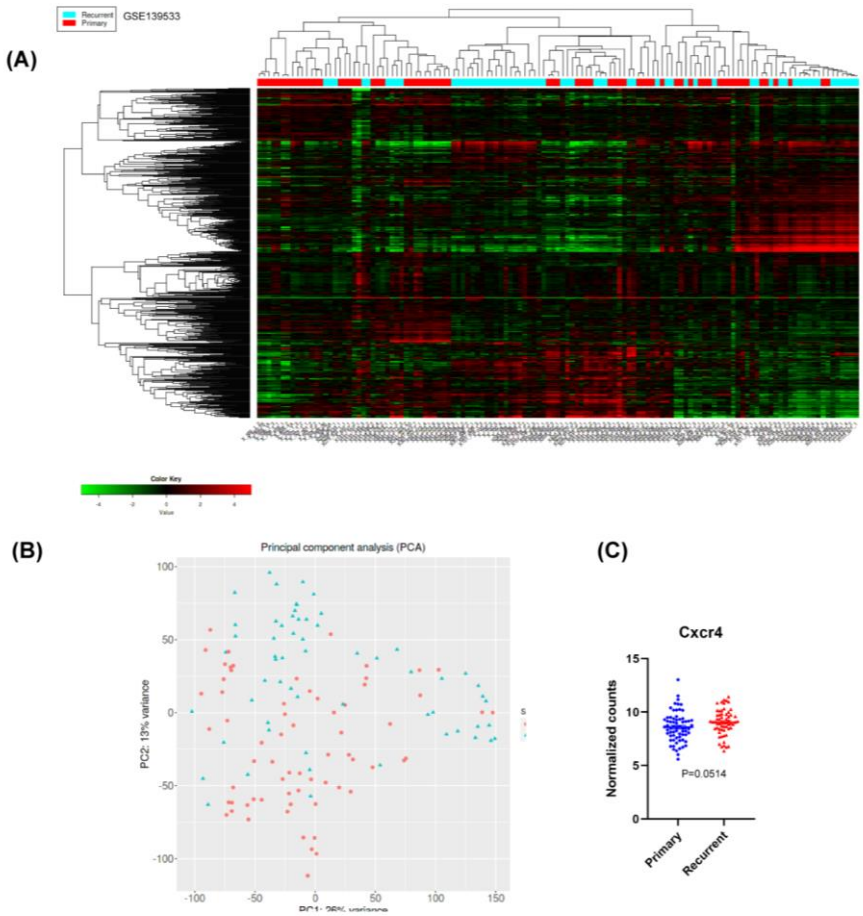

Figure 12. Reanalysis of gene expression profile GSE139533. (A) Heatmap of differentially expressed genes compared between primary and recurrent human GBM samples based on gene expression profile GSE139533 (n=47 paired samples). (B) Principal Component Analysis (PCA) plot of primary and recurrent human GBM. (C) Normalized counts of CXCR4 in paired primary and recurrent groups. *p=0.0514. Student's paired two-tailed t-test. Error bars represent mean ± s.e.m.

3.4 Effects of AMD3100 treatment on mutant NSCs *in vivo* and *in vitro*

Targeting the CXCL12/CXCR4 pathway following radiotherapy and temozolomide could improve the overall survival of patients with GBM. The recurrence pattern, however, may change in favor of an out-of-field pattern (58.8% out-of-field recurrences vs. 10% in a control group). Nevertheless, no studies have looked at how inhibiting the CXCL12/CXCR4 pathway right after complete resection affects local recurrence and prognostic survival in glioblastoma. Therefore, the pharmacological intervention was used with the particular CXCR4 blocker, Plerixafor (AMD3100), to examine the impact of blocking the CXCL12/CXCR4 chemokine axis in glioblastoma recurrence following complete resection. Following surgical resection, mice were treated with AMD3100 (1.25 mg/kg) or phosphate-buffered saline (PBS) as a control via intraperitoneal injection twice per day, with a 6-hour interval between injections. The use of AMD3100 allowed for the specific inhibition of CXCR4 signaling, which has been implicated in promoting the migration and invasion of cancer cells. After the final injection, the mice were sacrificed, and their brains were harvested for subsequent analyses. This experimental approach enables the investigation of the functional role of the CXCL12/CXCR4 axis in glioblastoma recurrence, and the use of a specific pharmacological blocker allows for the targeted modulation of this pathway in vivo. Blockade of the CXCL12/CXCR4 axis led to a reduction in the number of migrating oligodendrocyte progenitor cells (OPCs) and improved tumor control and survival rates (Figure 13 A-E). To investigate the effect of CXCR4 blockade on NSC differentiation, we generated neurosphere from NSCs of LSL-EGFRviii f/+; LSL-Cas9-GFP f/+ mice after Introducing cancer-driving mutations (Figure 13F-J). After treatment of AMD3100 on the NSC culture, the cells were immune-stained and processed for analysis of lineage differentiation (Figure 13K). While OPCs were the dominant subtype of differentiation in the control group, the addition of AMD3100 resulted in a decrease in the number of OPCs and preferential differentiation to astrocytes with GFAP positivity. It suggests that the CXCR4 blockade might have an effect on the differentiation of

NSCs and prevent OPC differentiation, a major pathway to tumor reconstruction (Figure 13L). These results suggest that blocking CXCL12/CXCR4 may be a potential therapeutic strategy for preventing local recurrences driven by residual NSCs after surgical resection of the primary tumor.

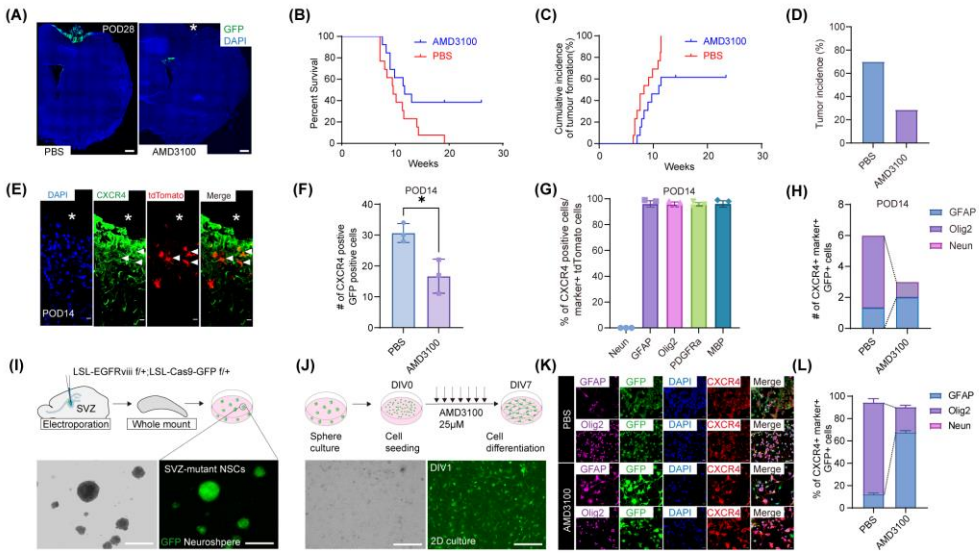

Figure 13. CXCL12/CXCR4 blockade treatment decreased the number of immigrating OPC lineage cells and improved survival in mice. (A) Representative images of local tumor development in the AMD3100 treatment group compared with the PBS group after 28 days of surgical resection (n=3 mice in each group). Scale bars, 500 μm. (B) Kaplan–Meier survival graph of mice (n= 13 mice in each group). p=0.0356, log-rank test. (C) Cumulative incidence of tumor incidence of mice (n=13 in each group). p=0.0256, log-rank test. (D) Comparison of tumor incidence in SVZ-mutated, AMD3100 treatment, and PBS group. Scale bars, 500 μm. (E) Representative images of GFP positive cells around RC after migrating from SVZ at POD14 of surgical resection. (F) Quantification of GFP-positive migrating cells around RC after AMD3100 treatment versus PBS group post 14 days of surgical resection (n=3 mice in each group). Student's two-tailed t-test. Error bars represent mean ± s.e.m. *p < 0.05. (G) Quantification of CXCR4 positive cells in migrating tdTomato positive cells around RC at 14 days after resection. (H) Quantification of various staining marker numbers

of CXCR4 positive migrating cells around RC after AMD3100 and PBS treatment post 14 days of surgical resection, including astrocyte marker GFAP, oligodendrocyte lineage cell marker OLIG2, and neuron marker NeuN (n=3 mice in each group). (I&J), Representative images of undifferentiated tumorsphere and differentiated monolayer cells growth after one day of incubation. SVZ-mutated cells were isolated and seeded in a confocal culture dish with triplicates. (K) Immunostaining images of GFAP and OLIG2 in cells after seven days treated with AMD3100 compared with PBS as a control. (L) Quantification of CXCR4 positive cells double-staining with GFAP, OLIG2, and NeuN in AMD3100 treatment versus PBS group after seven days of differentiation.

Chapter 5. Discussion

GBM is the most aggressive primary brain tumor with a poor prognosis despite diverse treatment options, including surgical resection, radiation therapy, and chemotherapy. Surgical resection is the mainstay of GBM therapy, but it has been suggested that surgical resection may contribute to GBM recurrence(46, 47). NSCs in SVZ were proved to be the cells of origin that contain the driver mutations of GBM(13). Our study provides novel evidence indicating that residual NSCs harboring cancer-driving mutations in the SVZ may be responsible for local recurrence formation at the RC after surgical resection of GBM (Figure 14).

Unlike previous studies that utilized xenograft models(46-48), our model ensures complete clearance of residual tumor cells around the RC after surgical removal. Various techniques have been developed to detect residual cells and remove them, but none of them guarantees the complete elimination of all residual cells. Thus, our model overcomes this limitation and allows us to study the relationship between NSCs and surgery without the confounding effect of in-situ recurrence of residual tumor cells. Remarkably, our model employs a subtle dual-color reporting system, which enables us to visualize tumor evidence derived from cancer-mutant NSCs even after the removal of the primary tumor. This observation provides important insights into the potential role of NSCs in tumor recurrence and underscores the importance of investigating NSC behavior in GBM recurrence and developing targeted therapy.

It has been suggested that brain injury and wound response may drive the progression of glioblastoma(37). Our findings identified NSCs in the SVZ as a potential origin of recurrence initiation that re-seed the RC in response to surgical resection, consistent with this hypothesis. Notably, the migration of stem cells has been identified in cases of traumatic brain injury, ischemia, and demyelination(49). However, there is a higher risk of increased neoplastic transformation only during traumatic brain injury(50). Therefore, our observations shed light on the potential role of NSCs in tumor

recurrence and emphasize the importance of investigating NSC behavior in the context of surgical resection in GBM recurrence.

In order to identify the underlying molecular mechanism of the biological action of tumor-initiating NSCs in SVZ responding to surgical resection, we collected time-course samples from the RC area in a genome-editing mouse model after surgical resection and applied them for RNA sequencing. It's interesting to note that, as early as POD2, cytokines continued to increase during local reconstruction and then maintained their elevated levels. This finding was consistent with previous reports of chemokines playing a crucial role in tumor progression and metastasis.

Of these genes, CXCR4 was the top up-regulated chemokine-associated gene during the recurrence process, which has been described as an essential chemokine driving the migration of NSCs toward the injury site after traumatic brain injury(51, 52). Previous studies(53-55) investigating CXCR4 blockade in GBM have primarily focused on inhibiting primary tumor growth or addressing treatment resistance rather than the local recurrence driven by SVZ after primary tumor resection. However, our study suggests that the recurrence of tumors induced by cancer-mutant NSCs in the SVZ may be attributed to an increase in CXCR4 expression.

Our findings indicate that CXCR4 is involved in the differentiation of mutant NSCs towards the OPC lineage, which was consistent with the studies showing that CXCR4 could promote the differentiation of oligodendrocyte progenitors into oligodendrocytes in the process of remyelination of the injured adult CNS(56). In our mouse model, OPC lineage was the dominant cell type during the reconstruction of glioma at RC, indicating with clonal evolution process of mutant NSCs migrating specifically to the RC through OPC lineage. Some studies also report mutated NSCs in SVZ contributed to glioma through aberrant growth of OPC lineage(12, 13, 57).

The fate of SVZ-NSCs is determined by both inherent characteristics and external factors, along with variations within the different regions of the SVZ (58, 59). In our model, there was no difference in the dominant lineage of migrating cells between SVZ-mutated NSCs and normal NSCs in the control group (data not shown). However, CXCR4 exhibits a higher

potential in influencing the commitment of oligodendrocyte progenitor cells compared to astrocytes, indicating its role in regulating the choice of glial lineage. To gain further insights into the relationship between lineage choice and sub-regional variations, it is crucial to conduct single-cell analysis of specific SVZ subregions involved in the regulation of astrocyte and oligodendrocyte production, incorporating specific factors. Such investigations would significantly contribute to our understanding of these processes, particularly within the context of surgical resection (59).

Thus, the high expression of CXCR4 not only led to the differentiation of NSC into OPC but also sustained high expression of CXCR4 during the differentiation and migration of OPC, which ensured the continuous progression to RC and eventually the reconstruction of glioma at the RC site. In addition, blocking CXCL12/CXCR4 by AMD3100 reduces the expression of OPC lineage cell markers *in vitro*, supporting the notion that increased CXCR4 expression in NSCs can promote their migration and differentiation. Furthermore, CXCR4/CXCL12 blockade by AMD3100 reduced tumor development and death rates in mice with mutated residual NSCs in the SVZ. Notably, we found high levels of CXCR4 in all local recurrent tumors from GBM human patients after gross total resection, highlighting CXCL12/CXCR4 as a promising target for GBM treatment. The phase I/II trial (NCT01977677) demonstrated some promising results for AMD3100 in glioblastoma treatment but has certain limitations (60,61). The study primarily focused on the effects of AMD3100 on macrophage exclusion after radiation therapy, with limited investigation of its role in inhibiting NSC-driven GBM recurrence after surgical resection. To advance our research, a more focused Phase II clinical trial should be conducted to evaluate the effectiveness and safety of AMD3100 as adjuvant therapy in GBM patients after gross total resection (GTR). This trial should assess primary endpoint with local recurrence free survival (LCFS) at six months and secondary endpoint including median survival, toxicities, and patterns of failure. Such a study would provide valuable insights into the potential benefits of AMD3100 added before standard treatment in improving outcomes for GBM patients after complete surgical resection.

Identifying NSCs as potential targets for preventing the recurrence of GBM underscores the importance of identifying target cells to develop effective targeted therapies. Our findings suggest that NSCs may be a viable target for preventing recurrence after surgical resection, which could help develop novel treatment strategies for glioma patients. We also underscore the importance of understanding the residual origin of solid cancer after primary treatments and its relationship with primary treatment. Further research is necessary to develop novel therapies targeting the residual origins of cancer.

Chapter 6. Conclusion

This study aimed to investigate the role of residual tumor-initiating neural stem cells (NSCs) in the subventricular zone (SVZ) in glioma recurrence after surgical resection. To this end, a mouse model with cancer-driving mutations in SVZ NSCs was developed. The migration of these NSCs, via oligodendrocyte precursor cells (OPCs), to the resection cavity (RC) and their ability to reconstitute glioblastoma (GBM) around it after surgery were examined. RNA sequencing of matched mouse and human primary-recurrence GBM samples was conducted to identify potential molecular mechanisms underlying tumor recurrence. The results revealed up-regulation of CXCR4/CXCL12 in tumors at recurrence after surgical resection. The CXCR4 antagonist AMD3100 was used to investigate the role of the CXCR4/CXCL12 pathway in glioma recurrence. AMD3100 was found to inhibit the differentiation of PROOPC lineages from NSCs and decrease their immigration to mouse RC. Furthermore, CXCR4/CXCL12 blockade reduced tumor development and death rates in mice with mutated residual NSCs in the SVZ. Taken together, these findings suggest that mutated residual NSCs in the SVZ may play a key role in tumor recurrence after surgical resection, and the CXCL12/CXCR4 pathway may be a promising treatment target for post-resection recurrence.

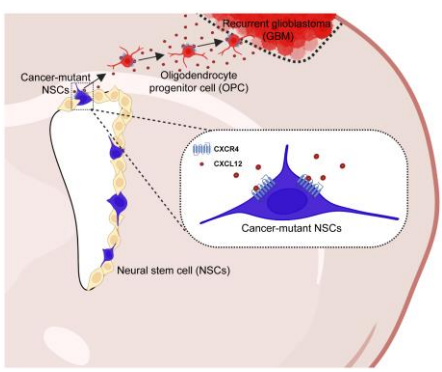

Figure 14. Graphical summary. A schematic showing the mechanism by which CXCR4/CXCL12 axis-mediated tumor-initiating NSCs in the SVZ migrate to the RC in glioblastoma recurrence.

Reference

1. Ostrom QT, Gittleman H, Farah P, Ondracek A, Chen Y, Wolinsky Y, et al. CBTRUS statistical report: Primary brain and central nervous system tumors diagnosed in the United States in 2006-2010. Neuro Oncol. 2013;15 Suppl 2(Suppl 2):ii1-56.
2. Louis DN, Perry A, Reifenberger G, von Deimling A, Figarella-Branger D, Cavenee WK, et al. The 2016 World Health Organization Classification of Tumors of the Central Nervous System: a summary. Acta Neuropathol. 2016;131(6):803-20.
3. Ostrom QT, Adel Fahmideh M, Cote DJ, Muskens IS, Schraw JM, Scheurer ME, et al. Risk factors for childhood and adult primary brain tumors. Neuro Oncol. 2019;21(11):1357-75.
4. Stupp R, Tonn JC, Brada M, Pentheroudakis G. High-grade malignant glioma: ESMO Clinical Practice Guidelines for diagnosis, treatment and follow-up. Ann Oncol. 2010;21 Suppl 5:v190-3.
5. Macdonald DR, Kiebert G, Prados M, Yung A, Olson J. Benefit of temozolomide compared to procarbazine in treatment of glioblastoma multiforme at first relapse: effect on neurological functioning, performance status, and health related quality of life. Cancer Invest. 2005;23(2):138-44.
6. Stupp R, Mason WP, van den Bent MJ, Weller M, Fisher B, Taphoorn MJ, et al. Radiotherapy plus concomitant and adjuvant temozolomide for glioblastoma. N Engl J Med. 2005;352(10):987-96.
7. Oh J, Sahgal A, Sanghera P, Tsao MN, Davey P, Lam K, et al. Glioblastoma: patterns of recurrence and efficacy of salvage treatments. Can J Neurol Sci. 2011;38(4):621-5.
8. Bette S, Barz M, Huber T, Straube C, Schmidt-Graf F, Combs SE, et al. Retrospective Analysis of Radiological Recurrence Patterns in Glioblastoma, Their Prognostic Value And Association to Postoperative Infarct Volume. Sci Rep. 2018;8(1):4561.

9. Rapp M, Baernreuther J, Turowski B, Steiger HJ, Sabel M, Kamp MA. Recurrence Pattern Analysis of Primary Glioblastoma. World Neurosurg. 2017;103:733-40.
10. Brandes AA, Tosoni A, Franceschi E, Sotti G, Frezza G, Amistà P, et al. Recurrence pattern after temozolomide concomitant with and adjuvant to radiotherapy in newly diagnosed patients with glioblastoma: correlation With MGMT promoter methylation status. J Clin Oncol. 2009;27(8):1275-9.
11. Alcantara Llaguno SR, Wang Z, Sun D, Chen J, Xu J, Kim E, et al. Adult Lineage-Restricted CNS Progenitors Specify Distinct Glioblastoma Subtypes. Cancer Cell. 2015;28(4):429-40.
12. Liu C, Sage JC, Miller MR, Verhaak RG, Hippenmeyer S, Vogel H, et al. Mosaic analysis with double markers reveals tumor cell of origin in glioma. Cell. 2011;146(2):209-21.
13. Lee JH, Lee JE, Kahng JY, Kim SH, Park JS, Yoon SJ, et al. Human glioblastoma arises from subventricular zone cells with low-level driver mutations. Nature. 2018;560(7717):243-7.
14. Alcantara Llaguno S, Chen J, Kwon CH, Jackson EL, Li Y, Burns DK, et al. Malignant astrocytomas originate from neural stem/progenitor cells in a somatic tumor suppressor mouse model. Cancer Cell. 2009;15(1):45-56.
15. Tomasetti C, Li L, Vogelstein B. Stem cell divisions, somatic mutations, cancer etiology, and cancer prevention. Science. 2017;355(6331):1330-4.
16. Ohgaki H, Kleihues P. The definition of primary and secondary glioblastoma. Clin Cancer Res. 2013;19(4):764-72.
17. Zheng H, Ying H, Yan H, Kimmelman AC, Hiller DJ, Chen AJ, et al. p53 and Pten control neural and glioma stem/progenitor cell renewal and differentiation. Nature. 2008;455(7216):1129-33.
18. Duan S, Yuan G, Liu X, Ren R, Li J, Zhang W, et al. PTEN deficiency reprogrammes human neural stem cells towards a glioblastoma stem cell-like phenotype. Nat Commun. 2015;6:10068.
19. Brennan CW, Verhaak RG, McKenna A, Campos B, Noushmehr H,

Salama SR, et al. The somatic genomic landscape of glioblastoma. Cell. 2013;155(2):462-77.

20. Killela PJ, Reitman ZJ, Jiao Y, Bettegowda C, Agrawal N, Diaz LA, Jr., et al. TERT promoter mutations occur frequently in gliomas and a subset of tumors derived from cells with low rates of self-renewal. Proc Natl Acad Sci U S A. 2013;110(15):6021-6.
21. Haskins WE, Zablotsky BL, Foret MR, Ihrie RA, Alvarez-Buylla A, Eisenman RN, et al. Molecular Characteristics in MRI-Classified Group 1 Glioblastoma Multiforme. Front Oncol. 2013;3:182.
22. Reynolds BA, Tetzlaff W, Weiss S. A multipotent EGF-responsive striatal embryonic progenitor cell produces neurons and astrocytes. J Neurosci. 1992;12(11):4565-74.
23. Craig CG, Tropepe V, Morshead CM, Reynolds BA, Weiss S, van der Kooy D. In vivo growth factor expansion of endogenous subependymal neural precursor cell populations in the adult mouse brain. J Neurosci. 1996;16(8):2649-58.
24. Doetsch F, Petreanu L, Caille I, Garcia-Verdugo JM, Alvarez-Buylla A. EGF converts transit-amplifying neurogenic precursors in the adult brain into multipotent stem cells. Neuron. 2002;36(6):1021-34.
25. Wechsler-Reya R, Scott MP. The developmental biology of brain tumors. Annu Rev Neurosci. 2001;24:385-428.
26. van Lookeren Campagne M, Gill R. Tumor-suppressor p53 is expressed in proliferating and newly formed neurons of the embryonic and postnatal rat brain: comparison with expression of the cell cycle regulators p21Waf1/Cip1, p27Kip1, p57Kip2, p16Ink4a, cyclin G1, and the proto-oncogene Bax. J Comp Neurol. 1998;397(2):181-98.
27. Gil-Perotin S, Marin-Husstege M, Li J, Soriano-Navarro M, Zindy F, Roussel MF, et al. Loss of p53 induces changes in the behavior of subventricular zone cells: implication for the genesis of glial tumors. J Neurosci. 2006;26(4):1107-16.
28. Sanai N, Alvarez-Buylla A, Berger MS. Neural stem cells and the origin of gliomas. N Engl J Med. 2005;353(8):811-22.
29. Alvarez-Palazuelos LE, Robles-Cervantes MS, Castillo-Velazquez G,

Rivas-Souza M, Guzman-Muniz J, Moy-Lopez N, et al. Regulation of neural stem cell in the human SVZ by trophic and morphogenic factors. Curr Signal Transduct Ther. 2011;6(3):320-6.

30. Nicoleau C, Benzakour O, Agasse F, Thiriet N, Petit J, Prestoz L, et al. Endogenous hepatocyte growth factor is a niche signal for subventricular zone neural stem cell amplification and self-renewal. Stem Cells. 2009;27(2):408-19.
31. Caporaso GL, Lim DA, Alvarez-Buylla A, Chao MV. Telomerase activity in the subventricular zone of adult mice. Mol Cell Neurosci. 2003;23(4):693-702.
32. Ferrón S, Mira H, Franco S, Cano-Jaimez M, Bellmunt E, Ramírez C, et al. Telomere shortening and chromosomal instability abrogates proliferation of adult but not embryonic neural stem cells. Development. 2004;131(16):4059-70.
33. Ohba S, Yamada Y, Murayama K, Sandika E, Sasaki H, Yamada S, et al. c-Met Expression Is a Useful Marker for Prognosis Prediction in IDH-Mutant Lower-Grade Gliomas and IDH-Wildtype Glioblastomas. World Neurosurg. 2019;126:e1042-e9.
34. Renault VM, Rafalski VA, Morgan AA, Salih DA, Brett JO, Webb AE, et al. FoxO3 regulates neural stem cell homeostasis. Cell Stem Cell. 2009;5(5):527-39.
35. Qian Z, Ren L, Wu D, Yang X, Zhou Z, Nie Q, et al. Overexpression of FoxO3a is associated with glioblastoma progression and predicts poor patient prognosis. Int J Cancer. 2017;140(12):2792-804.
36. Spiteri I, Caravagna G, Cresswell GD, Vatsiou A, Nichol D, Acar A, et al. Evolutionary dynamics of residual disease in human glioblastoma. Ann Oncol. 2019;30(3):456-63.
37. Richards LM, Whitley OKN, MacLeod G, Cavalli FMG, Coutinho FJ, Jaramillo JE, et al. Gradient of Developmental and Injury Response transcriptional states defines functional vulnerabilities underpinning glioblastoma heterogeneity. Nat Cancer. 2021;2(2):157-73.
38. Guo P, Xiao X, El-Gohary Y, Paredes J, Prasadan K, Shiota C, et al. A simplified purification method for AAV variant by polyethylene glycol

aqueous two-phase partitioning. Bioengineered. 2013;4(2):103-6.
39. Platt RJ, Chen S, Zhou Y, Yim MJ, Swiech L, Kempton HR, et al. CRISPR-Cas9 knockin mice for genome editing and cancer modeling. Cell. 2014;159(2):440-55.
40. Chow RD, Guzman CD, Wang G, Schmidt F, Youngblood MW, Ye L, et al. AAV-mediated direct in vivo CRISPR screen identifies functional suppressors in glioblastoma. Nat Neurosci. 2017;20(10):1329-41.
41. Kim D, Langmead B, Salzberg SL. HISAT: a fast spliced aligner with low memory requirements. Nat Methods. 2015;12(4):357-60.
42. Liao Y, Smyth GK, Shi W. featureCounts: an efficient general purpose program for assigning sequence reads to genomic features. Bioinformatics. 2014;30(7):923-30.
43. Love MI, Huber W, Anders S. Moderated estimation of fold change and dispersion for RNA-seq data with DESeq2. Genome Biol. 2014;15(12):550.
44. Subramanian A, Tamayo P, Mootha VK, Mukherjee S, Ebert BL, Gillette MA, et al. Gene set enrichment analysis: a knowledge-based approach for interpreting genome-wide expression profiles. Proc Natl Acad Sci U S A. 2005;102(43):15545-50.
45. Yu G, Wang LG, Han Y, He QY. clusterProfiler: an R package for comparing biological themes among gene clusters. Omics. 2012;16(5):284-7.
46. Okolie O, Bago JR, Schmid RS, Irvin DM, Bash RE, Miller CR, et al. Reactive astrocytes potentiate tumor aggressiveness in a murine glioma resection and recurrence model. Neuro Oncol. 2016;18(12):1622-33.
47. Knudsen AM, Halle B, Cédile O, Burton M, Baun C, Thisgaard H, et al. Surgical resection of glioblastomas induces pleiotrophin-mediated self-renewal of glioblastoma stem cells in recurrent tumors. Neuro Oncol. 2022;24(7):1074-87.
48. Otvos B, Alban TJ, Grabowski MM, Bayik D, Mulkearns-Hubert EE, Radivoyevitch T, et al. Preclinical Modeling of Surgery and Steroid Therapy for Glioblastoma Reveals Changes in Immunophenotype that

are Associated with Tumor Growth and Outcome. Clin Cancer Res. 2021;27(7):2038-49.

49. Chang EH, Adorjan I, Mundim MV, Sun B, Dizon ML, Szele FG. Traumatic Brain Injury Activation of the Adult Subventricular Zone Neurogenic Niche. Front Neurosci. 2016;10:332.
50. Tyagi V, Theobald J, Barger J, Bustoros M, Bayin NS, Modrek AS, et al. Traumatic brain injury and subsequent glioblastoma development: Review of the literature and case reports. Surg Neurol Int. 2016;7:78.
51. Saha B, Peron S, Murray K, Jaber M, Gaillard A. Cortical lesion stimulates adult subventricular zone neural progenitor cell proliferation and migration to the site of injury. Stem Cell Res. 2013;11(3):965-77.
52. Filippo TR, Galindo LT, Barnabe GF, Ariza CB, Mello LE, Juliano MA, et al. CXCL12 N-terminal end is sufficient to induce chemotaxis and proliferation of neural stem/progenitor cells. Stem Cell Res. 2013;11(2):913-25.
53. Calinescu AA, Yadav VN, Carballo E, Kadiyala P, Tran D, Zamler DB, et al. Survival and Proliferation of Neural Progenitor-Derived Glioblastomas Under Hypoxic Stress is Controlled by a CXCL12/CXCR4 Autocrine-Positive Feedback Mechanism. Clin Cancer Res. 2017;23(5):1250-62.
54. Alghamri MS, Banerjee K, Mujeeb AA, Mauser A, Taher A, Thalla R, et al. Systemic Delivery of an Adjuvant CXCR4-CXCL12 Signaling Inhibitor Encapsulated in Synthetic Protein Nanoparticles for Glioma Immunotherapy. ACS Nano. 2022;16(6):8729-50.
55. Tang W, Wang X, Chen Y, Zhang J, Chen Y, Lin Z. CXCL12 and CXCR4 as predictive biomarkers of glioma recurrence pattern after total resection. Pathol Biol (Paris). 2015;63(4-5):190-8.
56. Patel JR, McCandless EE, Dorsey D, Klein RS. CXCR4 promotes differentiation of oligodendrocyte progenitors and remyelination. Proc Natl Acad Sci U S A. 2010;107(24):11062-7.
57. Galvao RP, Kasina A, McNeill RS, Harbin JE, Foreman O, Verhaak RG, et al. Transformation of quiescent adult oligodendrocyte precursor cells into malignant glioma through a multistep reactivation process. Proc

Natl Acad Sci U S A. 2014;111(40):E4214-23.

58. David-Bercholz J, Kuo CT, Deneen B. Astrocyte and Oligodendrocyte Responses From the Subventricular Zone After Injury. Front Cell Neurosci. 2021;15:797553.
59. Mizrak D, Levitin HM, Delgado AC, Crotet V, Yuan J, Chaker Z, et al. Single-Cell Analysis of Regional Differences in Adult V-SVZ Neural Stem Cell Lineages. Cell Rep. 2019;26(2):394-406 e5.
60. Brown JM, Thomas R, Nagpal S, Recht L. Macrophage exclusion after radiation therapy (MERT): A new and effective way to increase the therapeutic ratio of radiotherapy. Radiother Oncol. 2020;144:159-64.
61. Thomas RP, Nagpal S, Iv M, Soltys SG, Bertrand S, Pelpola JS, et al. Macrophage Exclusion after Radiation Therapy (MERT): A First in Human Phase I/II Trial using a CXCR4 Inhibitor in Glioblastoma. Clin Cancer Res. 2019;25(23):6948-57.

국문초록

교모세포종에서 돌연변이를 갖는 신경줄기세포 기원의 재발 기전 연구

리슈에

서울대학교 대학원

의학과 방사선종양학 전공

서론: 교모세포종은 불량한 예후를 보이는 원발성 악성 뇌종양이며, 현재 표준 치료는 최대 국소 절제 후 방사선치료와 테모졸로마이드의 병용요법이다. 그러나 완전 절제에도 불구하고, 재발의 약 85%가 원발 종양의 절제 부위에서 발생하여 좀 더 효과적인 치료가 필요함을 시사한다. 최근 연구에 따르면 뇌실하 영역의 신경 줄기 세포가 교모세포종의 기원이라는 보고가 있다. 교모세포종 재발에 대한 신경 줄기 세포의 관여 여부 및 분자생물학적 기전은 아직 명확하지 않으나, 재발을 예방하기 위해 뇌실하 영역에 방사선치료를 시행하는 것이 제안되고 있다. 따라서 교모세포종 재발에 있어서 신경 줄기 세포의 역할에 대한 분자·세포 생물학적 메커니즘을 규명하기 위한 연구가 필요하다.

방법: 교모세포종에서 뇌실하 영역에 있는 암 유발 돌연변이를 가진 신경 줄기 세포의 역할을 확인하기 위해 유전자 변형 마우스 모델을 제작하였다. 생체 전기천공법을 통해 EGFR, TP53 및 PTEN 돌연변이를 마우스 뇌실하

영역의 신경 줄기 세포에 유발하였으며, 대뇌피질 절제술을 시행하였다. 이후 마우스 모델로부터 조직을 얻어 면역화학염색 및 RNA 염기서열분석을 진행하였다. 인간 교모세포종 환자의 조직을 사용하여 차등 발현 유전자군과 경로를 확인 및 입증하였다. 추가적인 생물학적 기능은 *in vitro* 및 *in vivo* 실험을 통해 확인하였다.

결과: 유전자 변형 마우스 모델 연구 결과, 뇌실하 영역의 암 유발 돌연변이를 가진 신경 줄기 세포가 희소돌기아교세포-전구세포로의 비정상적인 분화를 통해 절제강으로 선택적으로 이동하였다. 또한, 종양 절제 4주 후, 64.7% (11/17)의 마우스에서 절제강 주변으로 이동한 신경 줄기 세포로부터 교모세포종이 발생하였으며, 수술적 절제 후 발생하는 재발 종양을 모사함을 확인하였다. 해당 동물 모델의 뇌 절제 부위 주변에서 2일, 2주, 4주의 시간대별로 조직을 채취하여 조직 단위 RNA 염기서열분석을 진행하였으며, 이를 통해 CXCR4의 발현량이 종양을 절제한 2일 후부터 증가하여 종양의 재발 시점까지 높게 유지된다는 것을 확인하였다. 또한, 마우스 모델에서 절제강이 없는 원발성 종양과 비교하였을 때, 절제강이 있는 경우 신경 줄기 세포가 뇌실하 영역에서 절제강으로 이동하여 종양을 구축하는 동안에 CXCL12/CXCR4 케모카인 전달경로가 활성화된다. 56명의 교모세포종 재발 환자로부터 얻은 원발성 종양 및 재발 종양을 매칭하여 비교한 결과, 잔여 종양 증거가 없는 완전 절제 후 절제강 주위에서 국소 재발한 환자에서 기타 재발한 환자 (불완전한 절제 후 잔여 종양의 진행 및 두개강 내 다른 부위에서의 재발한 경우)에 비해 높은 CXCR4 발현을 확인하였다 (P=0.0176). 또한, CXCR4의 발현이 높은 국소 재발 환자는 불량한 예후를 보였다 (P=0.018). 마우스 모델에서 CXCL12/CXCR4 축의 약물적 차단은 절제강 내로 이동하는 신경 줄기 세포의 수를 줄였으며, 희소돌기아교세포-전구세포로의 분화를 억제하였다. 이를 통해 종국에는 종양 발생률을 감소시키고 생존률을 증가시켰다.

결론: 원발성 교모세포종의 수술적 제거 이후에, 뇌실하 영역의 암 유발

돌연변이를 내포한 신경 줄기 세포가 절제강에서의 재발의 원인이 되었다. CXCL12/CXCR4 경로는 이러한 신경 줄기 세포 기원의 재발을 억제하기 위한 중요한 타겟이 될 수 있을 것이다.

주요어: 교모세포종, 신경 줄기 세포, 재발, 희소돌기아교세포-전구세포, C-X-C 케모카인 수용체 type 4, 뇌실하 영역

학 번: 2018-35031